catalysts

MDPI

Article

Influence of Dopants on Pt/Al_2O_3-Based Monolithic Catalysts for Autothermal Oxidative Coupling of Methane

Sven Schardt, Simon Bastian, Ahmet Çelik, Jaspreet Chawla and Patrick Lott *

Institute for Chemical Technology and Polymer Chemistry (ITCP), Karlsruhe Institute of Technology (KIT), 76131 Karlsruhe, Germany; sven.schardt@kit.edu (S.S.); simon.bastian@kit.edu (S.B.); ahmet.celik@kit.edu (A.Ç.)
* Correspondence: patrick.lott@kit.edu

Abstract: Autothermal oxidative coupling of methane (OCM) is a highly attractive approach for methane utilization. If platinum-based catalysts are operated in short-contact-time reactors with high space velocities, high methane conversion can be achieved. Using a 1 wt.% Pt/Al_2O_3 catalyst as a benchmark, the present study elucidates how different dopants, namely Ni, Sn, and V_2O_5, affect the OCM reaction. Kinetic catalyst tests reveal that acetylene (C_2H_2) is the predominant C_2 product, irrespective of the catalyst formulation or operation conditions. Furthermore, the use of bimetallic catalysts allows either for the maintenance or even the improvement of the C_2 selectivity during OCM, which is attributed to synergistic effects that occur when expensive Pt is partially replaced by cheaper dopants. In particular, the 1 wt.% Pt/Al_2O_3 reference catalyst yielded a maximum C_2 selectivity of 8.2%, whereas the best-performing doped sample 0.25 wt.% Pt 0.75 wt.% V_2O_5/Al_2O_3 yielded a total C_2 selectivity of 11.3%.

Keywords: oxidative coupling of methane; doping; heterogeneous catalysis; gas-phase reactions; methane upgrading

check for updates

Citation: Schardt, S.; Bastian, S.; Çelik, A.; Chawla, J.; Lott, P. Influence of Dopants on Pt/Al_2O_3-Based Monolithic Catalysts for Autothermal Oxidative Coupling of Methane. *Catalysts* **2024**, *14*, 785. https://doi.org/10.3390/catal14110785

Academic Editors: Florica Papa, Anca Vasile and Gianina Dobrescu

Received: 8 October 2024
Revised: 25 October 2024
Accepted: 29 October 2024
Published: 5 November 2024

Copyright: © 2024 by the authors. Licensee MDPI, Basel, Switzerland. This article is an open access article distributed under the terms and conditions of the Creative Commons Attribution (CC BY) license (https://creativecommons.org/licenses/by/4.0/).

1. Introduction

With fossil resources depleting and increasing in cost, alternative sustainable approaches toward base chemicals are becoming more and more relevant [1]. In the context of hydrocarbon chemistry, methane (CH_4) as the simplest hydrocarbon is extremely versatile [2,3] and is therefore used in a wide variety of seminal applications, i.e., dry reforming for syngas synthesis or methane pyrolysis for H_2 production [4–7]. Although its high abundancy as the main component of natural gas [8] is currently limited due to geopolitical factors at least in Europe [9], sustainable processes such as the fermentation of biomass [1] or the conversion of excess renewable energies, e.g., from wind, solar, or water [10], into methane via so-called power-to-gas processes are feasible alternative CH_4 sources. Ultimately, CH_4 gained from these processes may allow independence from fossil resources and may likewise lead to a transition toward a renewable and green chemical economy.

The main challenge during methane utilization is the activation of the stable C-H bond of the symmetric CH_4 molecule, whose cleavage requires comparably high energy levels [8], which may be one of the main reasons that the vast majority of methane is exploited thermically during combustion processes [3]. However, proper catalytic systems can overcome this obstacle. For instance, by means of catalytic partial oxidation (CPOX, Equation (1)) [11] that commonly relies on catalysts based on platinum group metals (PGM) [11,12] or in some cases, also on Ni-based materials [13,14], methane is frequently converted into syngas (CO and H_2):

$$CH_4 + 0.5\ O_2 \rightarrow CO + 2\ H_2 \quad (1)$$

Subsequent processing, e.g., via the Fischer–Tropsch process, allows for the conversion of the obtained syngas into higher hydrocarbons like aliphates and alcohols [15]. Although

almost all industrially relevant (hydro)carbon-based compounds can be synthesized via this process chain, a process that directly yields higher-ordered hydrocarbon species without the necessity of an additional reaction step would be of both economic and ecological appeal, since reducing the number of process steps facilitates an efficient use of resources. In this regard, the oxidative coupling of methane (OCM) according to Equations (2)–(5) [16,17] is a promising approach to directly convert methane into C_2 species under oxidative conditions.

$$2\,CH_4 + 0.5\,O_2 \rightarrow C_2H_6 + H_2O \quad (2)$$

$$2\,CH_4 + O_2 \rightarrow C_2H_4 + 2\,H_2O \quad (3)$$

$$2\,CH_4 + 1.5\,O_2 \rightarrow C_2H_2 + 3\,H_2O \quad (4)$$

$$C_2H_6 + 0.5\,O_2 \rightarrow C_2H_4 + H_2O \quad (5)$$

As first discovered by Keller and Bhasin in 1982 [18], OCM couples two methane molecules to form C_2 species (Equations (2)–(4)). Equation (5) exemplarily shows a dehydrogenation step from ethane (C_2H_6) to ethylene (C_2H_4), which can occur at sufficiently high temperatures [19]. Lunsford [20] investigated these reactions and their underlying mechanism in more detail and found them to be highly dependent on both homogeneous and heterogeneous catalysis. Solid–gas interactions between the CH_4 molecule and the catalytically active surface sites weaken and ultimately split the C-H bond, resulting in $CH_3\bullet$ radicals that can then form C_2H_6 by recombination in the gas phase. A recent study by Zhou et al. [21] identified this radical formation capability as particularly crucial for a high activity of OCM catalysts.

Among the many materials that were suggested as suitable OCM catalysts, Mn-Na_2WO_4/SiO_2 is currently considered as one of the most active and hence promising formulations [22–25], since it allows for a C_2 yield of 20% and a maximum methane conversion of about 45% [22]. Analogous to other non-precious metal-based systems containing lanthanoids [26,27], alkali metals [28], or alkali earth metals [29], these catalysts mainly yield ethane and ethylene. However, further oxidative dehydrogenation (ODH) to the base chemical acetylene (C_2H_2) can further increase the product value and is therefore desirable. Vanadium pentoxide (V_2O_5) [30] and platinum (Pt) [31,32] have been reported as suitable materials for catalyzing the ODH of alkanes, and there are reports on a further activity increase in platinum upon doping with tin (Sn) or copper (Cu) [33]. Notably, the usage of platinum and rhodium as catalytically active materials for the OCM reaction as reported in 1998 by Hohn et al. [4] results in methane conversions well above 50% and most importantly directly yields C_2H_2, hereby offering a higher efficiency than non-noble metal-based materials. Herein, short contact times between the reaction gases and the foam-like, Pt-loaded monolithic substrate in the range of milliseconds resulted in high temperature levels and were a prerequisite for high activity and selectivity. Moreover, recent microkinetic studies by Chawla et al. [19,34] revealed gas-phase reactions occurring at high temperatures to be crucial for the formation of C_2 species for the platinum-catalyzed OCM (Pt-OCM). The interplay between support dopants and their impact on the $CH_3\bullet$ formation was investigated in a recent experimental study in our group [35].

Current C_2H_2 synthesis processes (e.g., calcium carbide technology or partial pyrolysis) commonly rely on high temperatures and therefore exhibit a high energy demand, which results in comparably high production costs [36,37]. Catalyst-based Pt-OCM at short contact times, on the other hand, offers the potential to directly yield acetylene during autothermal reactor operation; due to exothermic reactions catalyzed by platinum, the reaction sustains itself after a short ignition phase, without any further energy input [4,35]. Consequently, Pt-OCM is highly attractive in principle from an economic point of view; however, ensuring high catalyst durability and product selectivity remain challenging.

Since precious metals such as platinum are expensive and become progressively scarce, our present study investigates the effect of dopants on the Pt-OCM, with the aim to maintain high methane conversion and to achieve high C_2 product formation—in particular

aiming at a high C_2H_2 selectivity—while reducing the noble metal content. For this, Pt-X catalysts are prepared in different ratios with X as Ni, Sn, and V_2O_5, since these materials are commonly applied in several hydrocarbon reactions like ODH [30,33,38], CPOX [39,40], and OCM [40–42]. We elucidate the impact of the catalyst composition on the different product selectivities and aim at understanding the effect of dopants in such bimetallic systems, while keeping the overall metal loading of the catalyst constant. With regard to activity and selectivity, monometallic Pt-only catalysts serve as benchmark systems.

2. Results

2.1. Selectivity Toward C_2 Species

Figure 1 shows the total selectivity toward the C_2 products, namely C_2H_6, C_2H_4, and C_2H_2, as a function of the dilution (N_2 content in feed) for the different catalysts at a gas hourly space velocity (GHSV) of 458,000 h^{-1}. The data points at a dilution of 50 vol.% N_2 clearly demonstrate that the majority of the bimetallic catalysts achieve very similar selectivity levels as the 1 wt.% Pt/Al_2O_3 catalyst (black squares), while the 0.5 wt.% Pt/Al_2O_3 catalyst (orange circles) has the lowest total C_2 selectivity at this operating point. As at this dilution value the total C_2 selectivity is generally the highest, 50 vol.% N_2 is used as a general reference point in this study. Although the bimetallic samples have a lower noble metal content than the monometallic 1 wt.% Pt/Al_2O_3 catalyst, their selectivity is competitive for most of the formulations. Under consideration that the bimetallic samples with a Pt:X ratio of 1:3 contain only 0.25 wt.% Pt and nevertheless show higher C_2 selectivities than the 0.5 wt.% Pt/Al_2O_3 catalyst, we can conclude that the addition of suitable non-noble metal components can substantially reduce the need for precious metals without a relevant selectivity loss. Especially at higher dilutions (>55 vol.% N_2), these catalysts exhibit a higher C_2 selectivity compared to the monometallic samples and the catalysts with a Pt-X ratio of 3:1.

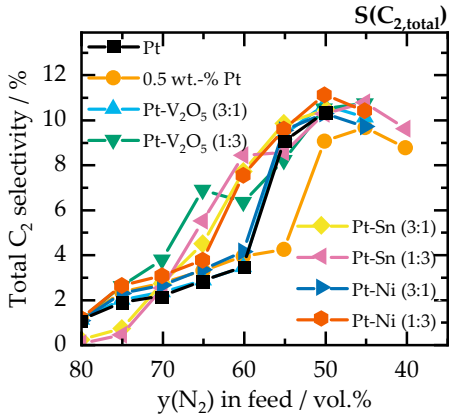

Figure 1. Total C_2 selectivity versus N_2 dilution for the investigated catalysts at 458,000 h^{-1} and a C:O ratio of 0.55.

Analyzing the contribution of different C_2 species to the overall C_2 selectivity at a dilution of 50 vol.% provides further insight into the different catalytic systems. Figure 2A shows the C_2H_2 selectivity for the catalysts subject to this study. The Ni-doped catalysts and the 1 wt.% Pt/Al_2O_3 reference catalyst exhibit the highest C_2H_2 selectivity (8.7%), followed by the V_2O_5-doped and the 0.5 wt.% Pt/Al_2O_3 catalyst (both about 8%). The lowest selectivity of approx. 7% was observed for the Sn-doped catalysts. Below a dilution of 50 vol.% N_2 in the feed, all catalysts show an identical behavior for all three C_2 products; solely Pt-Sn (3:1) extinguished when changing the operation parameters. With respect to the C_2H_4 selectivity (Figure 2B), the trends observed for the samples tested in this study differ. While the monometallic catalysts and the Ni-doped Pt-Ni (3:1) catalyst produce less C_2H_4 than the other formulations, a steep increase in C_2H_4 selectivity to approx. 6% is observed over Pt-Sn (1:3) and Pt-V_2O_5 (1:3) at a N_2 feed content as high as 55 vol.%. A

further decrease in the dilution causes a drop in C_2H_4 selectivity to levels similar to the other catalysts, and C_2H_2 selectivity increases steeply. Analogously, the maximum C_2H_6 selectivity of almost 2% over Pt-Sn (1:3) and Pt-V_2O_5 (1:3) at a N_2 dilution of 55 vol.% clearly exceeds that of the other catalyst samples, which show a continuous decline from a level as low as 0.5% for a N_2 content of 80 vol.% to almost zero at 50 vol.% dilution and below (Figure 2C).

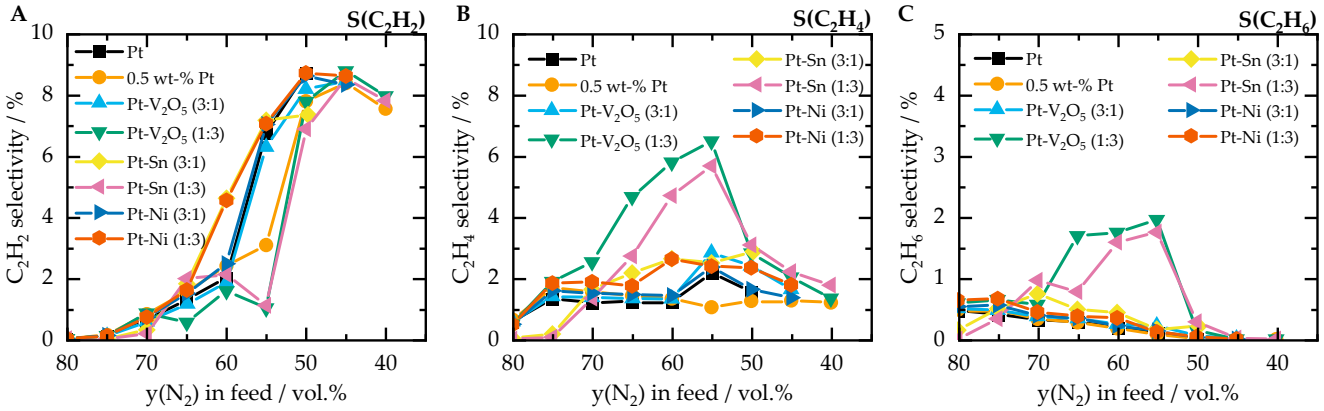

Figure 2. The selectivity toward the different C_2 species C_2H_2 (**A**), C_2H_4 (**B**), and C_2H_6 (**C**) at a GHSV of 458,000 h^{-1} and a C:O ratio of 0.55.

Using the data point with a N_2 content of 50 vol.% as a reference point, we can conclude that in terms of C_2 selectivity, the 0.5 wt.% Pt/Al_2O_3 catalyst shows the worst performance among the tested samples. Notably, the overall C_2 selectivities in general (Figure 1) and the C_2H_2 selectivities in particular (Figure 2A) are similar for all doped catalysts and the 1 wt.% Pt/Al_2O_3 sample, although the Pt-X (1:3) catalysts contain only 0.25 wt.% Pt. Hence, catalysts with a Pt–dopant ratio of 1:3 offer the greatest potential for saving scarce and expensive noble metals, while maintaining the selectivity level.

Since the space velocity also plays a crucial role in product selectivity, further tests were carried out at a lower GHSV of 295,000 h^{-1} to investigate the Pt-X (1:3) catalysts in more detail. Figure 3A depicts the total C_2 selectivity at a space velocity of 295,000 h^{-1} for the 1 wt.% Pt/Al_2O_3 and the 0.5 wt.% Pt/Al_2O_3 sample as well as for the three Pt-X (1:3) catalysts. All of them clearly exceed the performance of both monometallic catalysts irrespective of the dilution with N_2. The onset of C_2 species formation of the best-performing catalyst Pt-V_2O_5 (1:3) is found at 80 vol.% N_2, whereas 0.5 wt.% Pt/Al_2O_3 shows the lowest selectivity and the formation of C_2 species only starts at $y(N_2) < 60$ vol.%. Furthermore, the Ni-containing catalyst behaves similarly to the 1 wt.% Pt/Al_2O_3 catalyst in the beginning, starting to produce C_2 species at 65 vol.% N_2 dilution, but outperforming the monometallic catalyst especially for lower dilution values.

Moreover, Figure 3B shows the composition of the total C_2 selectivity at a 50 vol.% dilution and a space velocity of 295,000 h^{-1}. In all cases, the most versatile and valuable C_2 species, C_2H_2, is the main C_2 product, with each catalyst yielding a C_2 share of at least 80% C_2H_2 (based on the total C_2 selectivity). Since the C_2H_6 selectivity was always lower than 0.3%, it is not considered for the diagram depicted in Figure 3B.

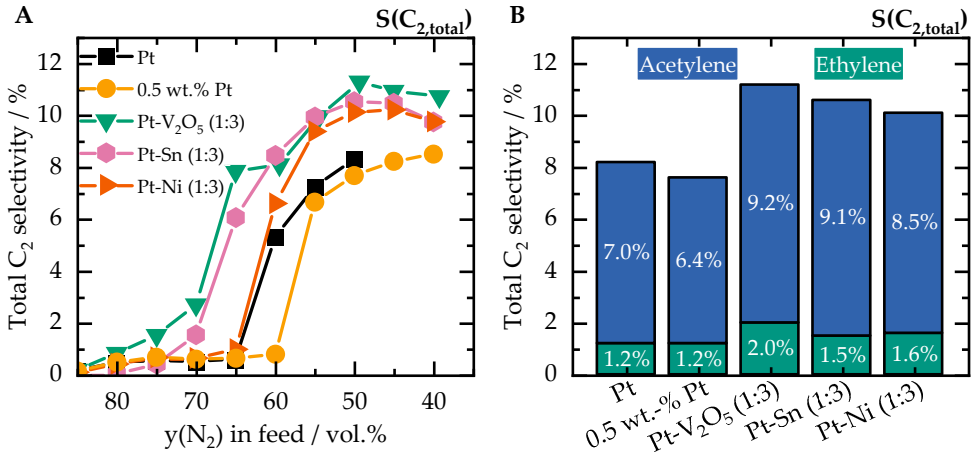

Figure 3. (**A**) Total C_2 selectivity against the nitrogen content in the feed at a GHSV of 295,000 h^{-1} and a C:O ratio of 0.55. (**B**) The composition of the C_2 selectivity for the catalysts shown in (**A**) at a dilution of 50 vol.%. Negligible C_2H_6 selectivities of less than 0.3% were found and are therefore not considered in the graph.

2.2. Selectivity Toward Other Product Species

In addition to the C_2 species, other products are also formed. These are mainly byproducts of the OCM reaction such as H_2O and valuable CPOX products, namely CO and H_2 (Equation (1)). Figure 4 shows the selectivity toward CO and H_2O (A and B, respectively), the corresponding conversion of methane (C), and the temperature downstream of the catalyst sample (D) at a GHSV of 458,000 h^{-1}. These data reveal pronounced differences between the investigated catalyst formulations, among which the Sn-doped catalysts stand out in particular. Pt-Sn (1:3) by far shows the lowest CO selectivity when starting the reaction at 80 vol.% N_2 content in the feed, whereas the H_2O selectivity exceeds the other catalyst systems at almost all operation points. Furthermore, Pt-Sn (1:3) and the two other bimetallic Pt-X (1:3; X = V_2O_5, Ni) catalysts show the lowest CO selectivity over the dilution range. At the reference point (50 vol.% N_2), all catalysts exhibit comparable CO selectivities. The Pt-V_2O_5 (1:3) and both Sn-doped catalysts show the highest H_2O selectivity of all samples at 50 vol.% N_2 content in the feed. On the other hand, in the range of 80 vol.% to 50 vol.% dilution, both Pt-Ni samples behave like the 1 wt.% Pt/Al_2O_3 catalyst.

Overall, the most significant deviations in the H_2O selectivity are observed for high and moderate N_2 contents, whereas the values become more similar for all catalysts once the N_2 content falls below 50 vol.%. As a general observation, increasing the dopant content in the catalyst from (3:1) to (1:3) lowers the CO selectivity by roughly 10% for dilutions between 80 vol.% and 55 vol.%, whereas for the H_2O selectivity, such clear correlations could not be found.

These general trends remain identical for the measurements conducted at the lower space velocity of 295,000 h^{-1} (Figure 5A,B). Especially for Pt-V_2O_5 (1:3) and Pt-Sn (1:3), the trends for the different product selectivities look very similar for both investigated space velocities. Pt-Sn (1:3) exhibits a significantly lower CO selectivity at high N_2 dilutions, and Pt-V_2O_5 (1:3) shows a drop in CO selectivity at 60 vol.% N_2 in the feed (Figure 5A). For a GHSV of 295,000 h^{-1}, the H_2O selectivity of Pt-Sn (1:3) is exceptionally higher throughout the N_2 variation and comes close to the values of the other catalysts at low dilutions (<50 vol.%). Likewise, Pt-V_2O_5 (1:3) shows a steep increase in H_2O selectivity at 70 vol.% N_2 in the feed and exhibits selectivity levels similar to those of the other catalysts at dilutions lower than 45 vol.% for both investigated space velocities.

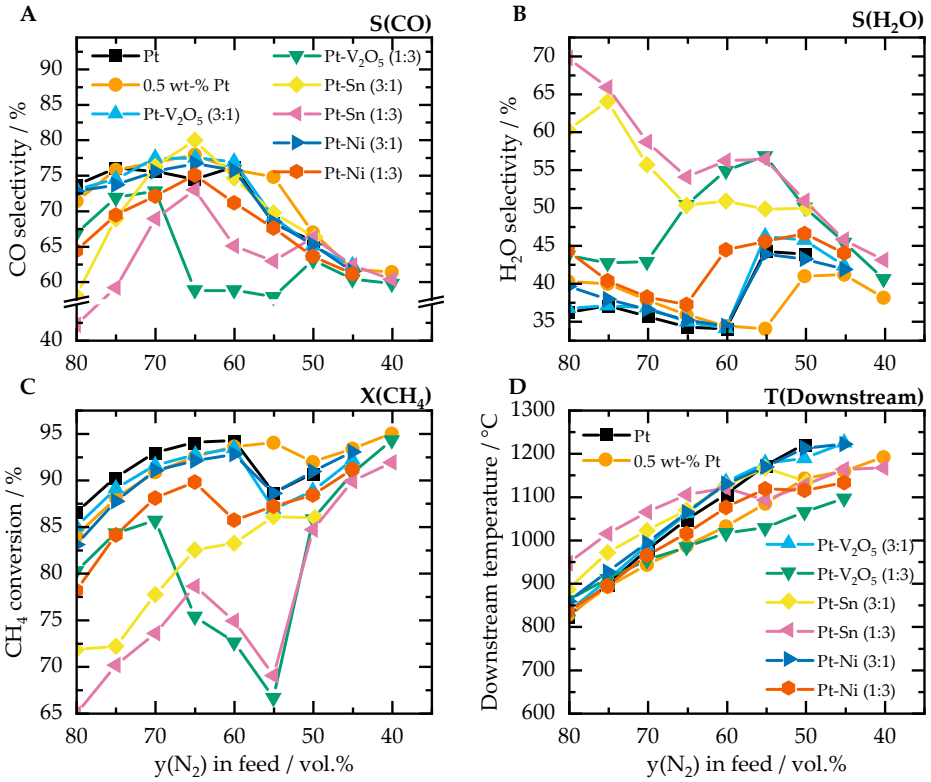

Figure 4. The measured selectivity toward CO (**A**) and H_2O (**B**), the methane conversion (**C**), and the downstream temperature (**D**) of the investigated catalysts, plotted versus the nitrogen content in the feed at GHSV of 458,000 h^{-1} and a C:O ratio of 0.55.

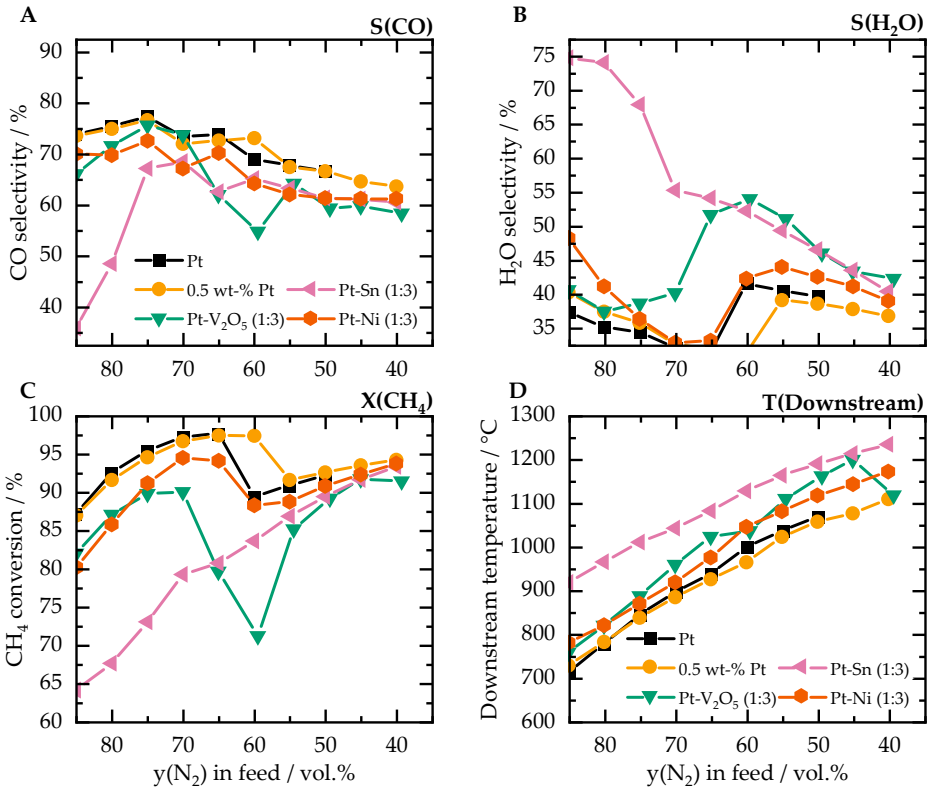

Figure 5. The measured selectivity toward CO (**A**) and H_2O (**B**), the methane conversion (**C**), and the downstream temperature (**D**) of the investigated catalysts, plotted versus the nitrogen content in the feed at GHSV of 295,000 h^{-1} and a C:O ratio of 0.55.

2.3. Methane Conversion and Temperature Evolution

Apart from the product selectivities, the conversion and temperature data can provide additional insights regarding the impact of dopants on Pt-OCM. Figure 4C correlates the methane conversion with the nitrogen content in the feed gas at a GHSV of 458,000 h^{-1}. While at 50 vol.% dilution the methane conversion values show a maximum deviation of ~7% and are therefore rather close to each other for every catalytic system, the trends differ at higher N_2 contents. Both tin-containing catalysts as well as the Pt-Ni and Pt-V_2O_5 (both 1:3) exhibit lower conversions than the monometallic catalysts and Pt-X (3:1; X = V_2O_5, Ni). In analogy to the trends observed for the CO selectivity, both Pt-Sn (1:3) and Pt-V_2O_5 (1:3) show a severe decrease in methane conversion at about 55 vol.% dilution, before their activity increases again when lowering the N_2 content further, hereby coming closer to the activity of the other catalysts at 50 vol.% dilution. Irrespective of the catalyst formulation, the product gas temperature measured 0.5 cm downstream the catalyst (Figure 4D) increases steadily with decreasing N_2 content. Only Pt-Sn (3:1) shows a temperature drop at 50 vol.% N_2 dilution, consistent with the selectivity and conversion drops observed at this dilution (Figure 4A,C). The reaction over Pt-V_2O_5 (1:3) results in the lowest temperature level, whereas the use of monometallic 1 wt.% Pt/Al_2O_3 results in the highest peak temperature. At 50 vol.% N_2 dilution, for instance, the gas temperature was determined to be 1064 °C for Pt-V_2O_5 (1:3) and 1220 °C for 1 wt.% Pt/Al_2O_3. Irrespective of the dilution, an almost total conversion was observed for oxygen.

Analogous to the CO and H_2O selectivity trends discussed in the previous section, the temperature trends are similar for the two space velocities (GHSV = 295,000 h^{-1} and 458,000 h^{-1}) tested within this study. The conversion of methane, for instance, increases by about 2–3% when lowering the GHSV (Figures 4C and 5C). While the decrease in conversion at about 60 vol.% N_2 and a GHSV of 458,000 h^{-1} is observed for the Pt-V_2O_5 (1:3) catalyst at 295,000 h^{-1} as well, Pt-Sn (1:3) exhibits this behavior only at a GHSV of 458,000 h^{-1}. Nevertheless, compared to the other catalysts, Pt-Sn (1:3) shows the lowest methane conversion of only 65% at high dilutions (vs. 80% for Pt-Ni (1:3), for instance, which shows the second-lowest conversion at 80 vol.% N_2 dilution). The temperature trend strongly depends on the catalyst formulation. While a change in space velocity does not change the temperature evolution of the Pt-Ni (1:3) catalyst, decreasing the space velocity from 458,000 h^{-1} to 295,000 h^{-1} leads to a steeper increase in temperature for Pt-X (1:3, X = Ni and V_2O_5) and a slower increase for the monometallic catalysts. This is also represented in absolute values at the reference point of 50 vol.% N_2 content. While the temperature level over Pt-Ni (1:3) is almost the same for both space velocities, 1 wt.% Pt/Al_2O_3 loses about 200 °C and Pt-V_2O_5 (1:3) is about 100 °C hotter when comparing the temperatures at a space velocity of 295,000 h^{-1} with those measured at 458,000 h^{-1}.

3. Discussion

The results presented above suggest that the introduction of dopants is a feasible strategy to reduce the noble metal content in OCM catalysts while maintaining an at least identical magnitude of selectivity toward the desired products C_2H_2 and C_2H_4 over all bimetallic catalyst samples. This is particularly remarkable since the Pt content was reduced by approx. 75% for the samples with a Pt:X ratio of 1:3. At a lower space velocity of 295,000 h^{-1}, the bimetallic catalysts even exceed the C_2 selectivity of the monometallic Pt catalyst. Possibly, this higher activity is enabled by facilitated CH_4 activation due to the presence of the dopants, which requires slightly higher residence times to be fully exploited.

Characterization data provide additional information on the different catalyst samples. The N_2 physisorption data (cf. Supporting Information, Table S4) demonstrate that all samples exhibit similar surface areas ($\geq$200 m^2/g) and pore volumes (approx. 0.5 cm^3/g). As the only exception, Pt-V_2O_3 (3:1) has a pore volume of approx. 0.4 cm^3/g that is slightly lower than any other catalyst. However, since this specific catalyst did not show exceptional results, we considered the effect of these structural parameters on the catalytic activity negligible for the materials subject to our study.

Furthermore, only reflections that are characteristic for the support material are visible in the XRD patterns of the fresh catalyst samples (Figure 6A), irrespective of the catalyst formulation. The absence of characteristic reflexes for the noble metal and the dopants point to either amorphous phases or, under consideration of the fairly low loading, more likely to a fine dispersion of the active materials. As underscored by the X-ray diffractograms shown in Figure 6B, the use of the catalysts under OCM conditions induces pronounced changes in the catalyst structure. On the one hand, the XRD data suggest a transformation of γ-Al_2O_3 into α-Al_2O_3, which typically takes place at temperatures above 1200 °C [43] as present during the OCM reaction. As demonstrated recently, such support-related transformations may be prevented by La doping of the support material [35]. On the other hand, noble metal-related reflexes also become visible, despite the lower data quality that is a consequence of the substantially lower sample amount available for characterization after exposure to OCM reaction conditions and that is possibly further impacted by contamination with small amounts of cordierite. Less than 50 mg of washcoat are coated onto a single monolithic sample, which needs to be removed from the cordierite substrate prior to XRD analysis. Reflexes, e.g., at 21.8° and 28.5°, are characteristic for PtO_2 [44], which suggests that the oxidative reaction conditions and high temperatures evolving during OCM cause a significant sintering of the Pt particles and their oxidation. Notably, the 0.5 wt.% Pt/Al_2O_3 catalyst shows the lowest Pt-related reflex intensities, although it is not the catalyst with the lowest Pt loading. Furthermore, a higher Pt loading results in more intense PtO_x reflexes for samples doped with V_2O_5 and Sn, whereas the diffractograms of the Ni-doped samples with high and low Pt loading strongly resemble each other. These findings point to an impact of the dopants on the noble metal, which supports implications of the catalyst performance data discussed in detail in the previous sections. In addition to differences in the particle sintering tendency and crystallinity, the dopants may also influence the oxidation state of the platinum and its reducibility, which is of particular relevance for the heterogeneous reactions taking place during OCM and should therefore be considered during future investigations that aim at substantiating such structure–activity correlations.

The above-mentioned phase change of the support material from γ-Al_2O_3 to α-Al_2O_3 is likely the reason for the drop in methane conversion and the corresponding drop in C_2H_2 selectivity as well as the increase in C_2H_4 and C_2H_6 selectivity that is observed when decreasing the dilution from 70 vol.% to 55 vol.%. At these dilution values, the catalysts reach sufficiently high temperatures (Figures 4 and 5D) for provoking a phase change. In this context, it is important to emphasize that the temperatures presented in this study were measured downstream of the catalyst. Consequently, the temperature inside the catalyst is expected to be much higher [4,34], which was also shown in a recent publication from our group [19]. Once a new, stable material phase evolves, the catalytic system returns to stable operation at a higher conversion level. Recently, we reported on similar trends for Pt/Al_2O_3-based samples operated under OCM conditions and found that the addition of 20 wt.% La_2O_3 to the γ-Al_2O_3 support material can suppress the influence of the phase change and thus the corresponding local activity minimum [35]. That this conversion and C_2H_2 selectivity minimum is most pronounced for Pt-V_2O_5 (1:3) and Pt-Sn (1:3) (Figure 2A–C) suggests that the dopants also undergo temperature-induced changes, as discussed in more detail below. However, heterogeneous reactions are only one aspect during OCM, because gas-phase chemistry is also believed to play an important role [19,20,34]. The temperature of the effluent reaction gas and the C_2 species yield correlate (cf. Supporting Information, Figure S1), as the formation of methyl radicals that can form C_2 species and the dehydrogenation reactions of C_2H_6 or C_2H_4 that may take place subsequently require sufficient amounts of thermal energy [4,21] and are therefore promoted by high reaction temperatures. Additionally, for these high temperatures, C_2H_2 is the thermodynamically favored product among the C_2 species [45].

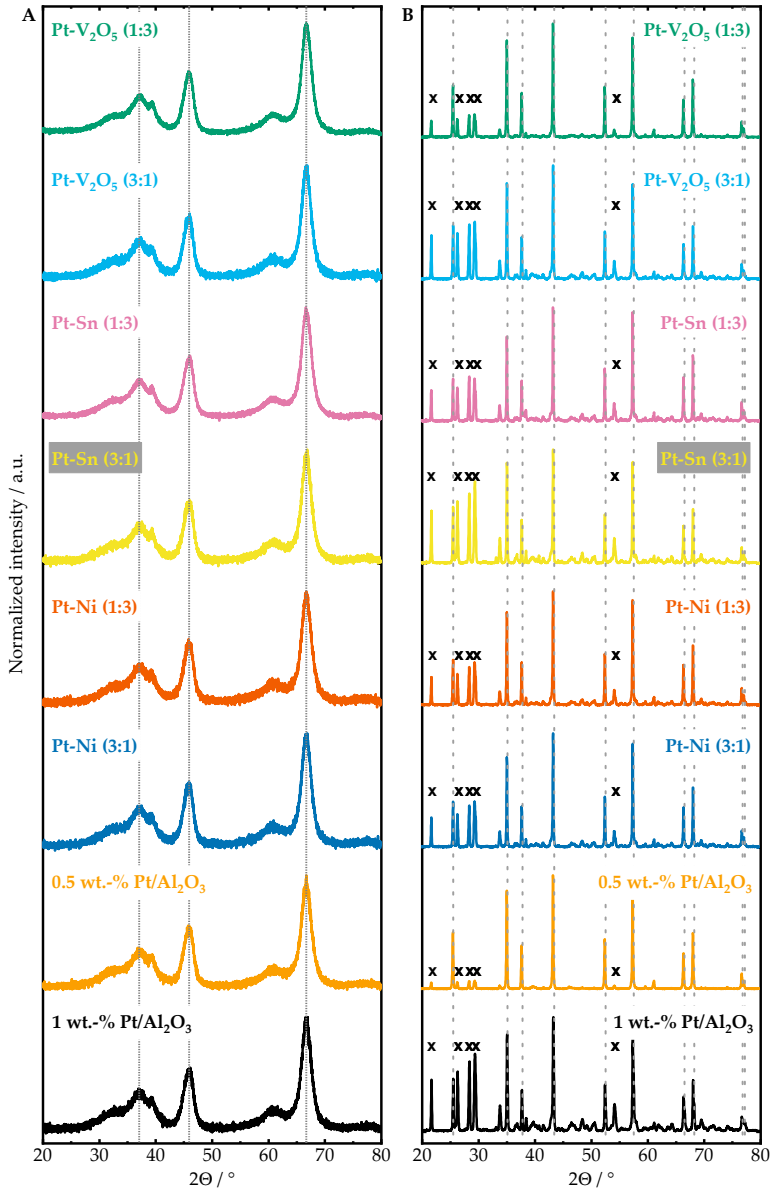

Figure 6. Comparison of the X-ray diffractograms of the different (**A**) fresh and (**B**) used catalysts of this study. The grey, compact lines in (**A**) show reflexes for γ-Al_2O_3; in (**B**), the grey, dotted lines mark α-Al_2O_3 reflexes and the x's mark reflexes of platinum oxides.

Notably, according to the data obtained at 458,000 h^{-1}, the best-performing catalyst Pt-V_2O_5 (1:3) shows an identical C_2 selectivity like the 1 wt.% Pt/Al_2O_3 catalyst, although the temperature ($T_{downstream}$) is about 160 °C lower (Figures 1 and 4D). This points to an active contribution of the V_2O_5 species within the typically Pt-governed OCM mechanism and underscores the importance of an interplay between heterogeneous reaction pathways governed by the catalyst material and gas-phase chemistry. We assume that the oxygen atoms in the vanadium pentoxide surface species play a crucial role. V_2O_5 is not only an excellent oxidation catalyst; i.e., it is vastly applied for oxidizing SO_2 to SO_3 during sulfuric acid production [46], but it is also a common choice for selective catalytic reduction (SCR) of nitrogen oxides with ammonia in the field of emission control [47,48], which was postulated to proceed via a V^{4+}/V^{5+} redox mechanism [49]. Analogously, the V_2O_5 surface species may interact with methane at comparably high temperatures during the OCM reaction, hereby facilitating scission of the C-H bond. Furthermore, the CO selectivity is lower than for the Pt-only catalyst. Since CO is a reaction product formed during partial oxidation of methane, a drop in CO selectivity also underscores a more pronounced methane consumption to form

C_2-coupling products during OCM reactions. These assumptions are supported by the fact that V_2O_5 is frequently used as a catalyst for the oxidative dehydrogenation of alkanes, where C-H bond cleavage plays an equally important role as in the field of OCM [30]. The drop in methane conversion observed at a N_2 content of 60 vol.% in the feed for both space velocities, 295,000 h^{-1} and 458,000 h^{-1}, might be due to changes in the valence state of vanadia [46]. For instance, Harlin et al. [50] reported a drop in the valence state from +5 to +4.1 when reducing a vanadium sample with CO at 580 °C. In the context of our results, the varying CO content in the product gas stream (i.e., Figures 4 and 5A) may influence the valence state of vanadium and therefore the catalytic activity. Moreover, Trunschke et al. [51] observed an increasing share of V^{5+} species when exposing MoV and a MoVTeNb mixed oxide catalysts used for the selective oxidation of lower alkanes to a humid reaction atmosphere. Hence, oxidation state variations of vanadium may account for the non-linear trend of the H_2O selectivity depicted in Figures 4 and 5B that directly correlates with CH_4 conversion (Figures 4 and 5C). After all, a decreasing N_2 dilution inevitably results in an increased content of reactive gases in the feed; therefore, the absolute amount of product species and the temperature typically increase (i.e., Figures 1 and 4D). Based on these results, we can speculate about an influence of both reaction gas mixture as well as temperature on the oxidation state of vanadia, which in turn influences the catalytic activity and may change the underlying OCM reaction mechanism.

While vanadium oxide-based catalysts exhibit a good stability under water-free conditions [52,53], humid conditions along with excess oxygen and elevated temperatures (750 °C) are known to result in high volatility of vanadia [52,54]. Considering the high reaction temperatures well above 1000 °C and the high water concentrations that are characteristic during OCM, V-doped catalysts are at risk to suffer from the low hydrothermal stability of vanadia in the long run. Interestingly, at least during our lab-scale catalyst tests, we did not observe a performance drop with time on stream, as after the dilution variation experiments (Figures 1 and 3, approximately 1.5 h of catalyst operation), both CH_4 conversion and C_2 selectivity remained high. However, according to the elemental analysis (cf. Supporting Information, Figure S2), at least some of the active species was lost during catalyst operation under OCM conditions, which increases the need for developing "anchoring" strategies capable of ensuring that the noble metal as well as the dopant remain on the support material for a long time. A rational catalyst and process design is of particular importance, also with regard to the oxidation state of vanadium, because the melting temperatures range from 677 °C for V_2O_5 [43] and up to 1967 °C for VO_2 [43]. Consequently, it would be interesting to evaluate the thermal stability of different V oxides along with their catalytic activity under harsh OCM conditions in future studies.

Since Ni and Pt are part of the same group in the periodic table, previous research aimed at substituting the more expensive platinum by nickel in various processes such as reforming reactions [55,56] or CPOX [14,15]. Our present results reveal a very similar behavior of the Pt-only and the Pt-Ni (1:3) samples under almost all experimental parameters investigated herein. At a space velocity of 295,000 h^{-1} and at lower dilutions, the Ni-containing catalyst even outperformed the 1 wt.%Pt/Al_2O_3 catalyst with respect to C_2 selectivity, hereby underscoring the suitability of Ni species for oxidative coupling of methane. Du et al. [57] recently reported that nickel can impact the oxidation state of platinum during the catalytic oxidation of toluene. Although in principle Ni shows activity for reforming reactions with methane [55], its influence on the oxidation state of platinum may play a crucial role as well and may govern both reactivity and selectivity. A recent publication by Ross [40] reviews and discusses the role of nickel in C_1 chemistry. First, nickel may interact with the alumina support to form nickel aluminate species and become reduced in the presence of hydrogen. In combination with the reactivity boost achieved when using bimetallic Pt-Ni phases in oxidative atmospheres [57], both the interaction between Pt and Ni as well as the interaction of Ni with the support could enhance the selectivity of our catalytic system.

Since according to the elemental analysis some nickel is lost during OCM operation (cf. Supporting Information, Figure S2), such an incorporation into the alumina support did likely not occur for our catalyst; this hypothesis is further supported by the XRD data, since the support-related reflexes would change if actual nickel aluminate would have formed. In fact, Pt-Ni alloys were reported to have potentially lower melting and boiling points than pure Ni, which may even facilitate the extraction of expensive Pt from the catalyst. On the other hand, NiO has a higher thermal stability than metallic Ni (melting temperature of 1453 °C for Ni [43] vs. melting temperature of 1984 °C for NiO [43]). Thus, the oxidative conditions that prevail during OCM may benefit the presence of more stable NiO. More advanced preparation techniques may offer a promising approach to evaluate if, along with Ni species, Pt could also be bound more strongly onto or into the support material. Such an incorporation could enhance the to date insufficient (hydro)thermal stability of Pt-based OCM catalysts and ultimately increase the industrial attractiveness of the OCM reaction.

As described in the context of the data plotted in Figures 4 and 5, the tin-containing catalysts exhibit higher water selectivity than the other systems that were subject to the present study. Since the high selectivity values are due to the comparably low methane conversion, absolute values are needed for comparison. In particular, at 295,000 h^{-1}, 50 vol.% N_2 dilution, and a C:O ratio of 0.55, 1 wt.% Pt/Al_2O_3, 0.5 wt.% Pt/Al_2O_3, Pt-Sn (1:3), Pt-V_2O_5 (1:3), and Pt-Ni (1:3) show absolute water concentrations of 9.5%, 9.3%, 10.8%, 10.8%, and 10.0%, respectively. These values in relation to the absolute values of C_2 species concentrations (cf. Supporting Information, Table S5) indicate a possible optimum in H_2O formation for high C_2 selectivity, as Pt has the lowest C_2 selectivity and both Pt-Sn (1:3) and Pt-V_2O_5 (1:3) show the highest selectivities. Considering that all the OCM reactions (Equations (2)–(5)) result in water as the product, we can conclude that doping with Sn results in a higher selectivity toward C_2 product formation. Moreover, results by Yokoyama et al. [33] point to a positive impact of tin on Pt-based dehydrogenation catalysts, since the formation of PtSn and Pt_3Sn alloys enhances the selectivity toward the ODH reaction. Ultimately, our kinetic data do not suggest a negative impact of chlorine ions from the precursors on the catalyst performance, e.g., as previously reported in the context of total oxidation of methane [58]. However, in terms of stability, Sn-containing samples suffered from an almost complete loss of Sn during OCM operation (cf. Supporting Information, Figure S2) and equally important, the loss of Sn seems to promote the loss of Pt as well, as approximately 50% of Pt was lost during an experimental run. This pronounced loss of active material may also correlate with the exceptionally high temperature that was observed during OCM operation, especially for Pt-Sn (1:3) for a space velocity of 295,000 h^{-1} (Figure 5D). Although these high temperatures benefit C_2 selectivity, the loss of active material makes Sn-containing catalysts unsuitable for long-term operation.

A general comparison of the CH_4 conversion and the product selectivity of doped samples with those of the monometallic ones (Figures 4 and 5) uncovers that the most pronounced differences occur if the dilution is moderate, i.e., $y(N_2) > 50$ vol.%. As the temperature steadily increases with decreasing N_2 dilution (Figures 4D and 5D), this effect may be attributed to the importance of gas-phase reactions. As already mentioned above, Chawla et al. [19] identified gas-phase reactions during Pt-OCM as an origin of methyl radicals, which are precursors for the desired C_2 products. Although their impact remains high, heterogeneous reaction pathways that are strongly influenced by the catalyst formulation may become less important at low dilutions, irrespective of the catalyst formulation. This becomes particularly clear when the overall similar trends of the C_2 selectivity data in Figures 1 and 2 are considered. Instead, gas-phase reactions become dominant, which could explain why the C_2 selectivities as well as CO and H_2O selectivities become increasingly similar over all catalyst samples when the N_2 content is lowered and the reaction temperature rises. Ultimately, the dopants added to the catalytic system may also offer the opportunity to prevail or achieve the postulated active oxidation state of Pt^0 for the (partial) oxidation of CH_4 [59,60] during the reaction and may thus improve both activity and selectivity of the catalysts.

4. Materials and Methods

4.1. Catalyst Preparation

Catalyst powders were prepared via incipient wetness impregnation (IWI) using γ-Al_2O_3 (Puralox, Sasol, Johannesburg, South Africa) that was calcined at 700 °C for 5 h in static air. For this, the platinum precursor $(NH_3)_4Pt(NO_3)_2$ (Alfa Aesar, Haverhill, MA, USA) was dissolved in deionized water (volume equal to the pore volume of the calcined alumina). The resulting solution was added in several steps to the support, and the received powder was dried at 80 °C for 4 h and subsequently calcined at 500 °C for 5 h in static air. Analogous to the procedure described by Karinshak et al. [61], the prepared powder catalyst was then coated onto a cordierite honeycomb monolith (1 cm length, 1 cm diameter, 400 cpsi, Corning, Corning, NY, USA). For this, the powder was mixed with deionized water and AlO(OH) (Disperal P2, Sasol) in a ball mill (Fritsch Pulverisette 6, Fritsch, Idar-Oberstein, Germany) at 300 rpm for 5 min twice with a 10 min break in between. The prepared slurry was then carefully coated onto the monolith until a metal loading of approximately 30 g ft^{-3} was reached. As last step, the coated monolith was calcined at 550 °C for 5 h.

For the nickel-containing powder catalysts, $Ni(NO_3)_2 \cdot 6H_2O$ (Alfa Aesar) was added to the impregnation solution, which allows for the simultaneous addition of Ni and Pt to the support. For the tin-containing catalysts, a second impregnation step with $SnCl_2 \cdot 2H_2O$ (Sigma Aldrich, St. Louis, MO, USA) dissolved in water was performed after drying the Pt/Al_2O_3 powder. Ammonium metavanadate (NH_4VO_3, Sigma Aldrich) was used as precursor for vanadium-containing samples. It was pretreated by heating in an oxalic acid solution (Merck, Darmstadt, Germany) until the solution changed its color from yellow to blue and was subsequently impregnated onto the dried (but not yet calcined) Pt/Al_2O_3 sample. These catalysts are denoted as Pt-V_2O_5, as this is the typical oxidation state of vanadium after catalyst preparation. After calcination of the bimetallic catalysts (5 h at 500 °C in static air), the powders were coated onto honeycombs as described before.

Unless stated otherwise, the powder catalysts exhibit a total active species loading of 1 wt.%. The nomenclature used in the following specifies the active material and the species ratio. The Pt-Ni (1:3) sample, for instance, contains 0.25 wt.% Pt and 0.75 wt.% Ni that are supported on γ-Al_2O_3.

4.2. Experimental Setup and Procedure

A detailed scheme of the setup used for the present study is depicted in Figure 7. The monolithic catalyst is placed inside a quartz glass tubular reactor with a length of 62.5 cm and an inner diameter of 2 cm; however, approximately 5 cm of the reactor is narrowed down to a diameter of 1 cm, which eases the loading with small monolithic catalyst samples. To improve heat transfer, a heat shield (length 1 cm, diameter 1 cm, uncoated cordierite monolith, 400 cpsi, Corning) is placed 0.5 cm upstream of the catalyst. The reactor is located inside a Carbolite HST 12/400 furnace (Carbolite Furnaces, Sheffield, UK) with a length of 40 cm. The reaction gases N_2, CH_4, and O_2 are dosed with mass flow controllers (MFCs, Bronkhorst, Ruurlo, The Netherlands) into the system and are premixed and preheated to 190 °C before entering the reactor. A ceramic-covered type S thermocouple about 0.5 cm downstream of the catalyst continuously monitors the exhaust gas temperature. The effluent gas stream itself flows through heated pipes (190 °C) into an online Fourier-transform infrared (FTIR) spectrometer (MultiGas 2030, MKS Instruments, Andover, MA, USA) that analyzes the gas composition once per second. Since the volume of the gas stream can change during the reaction, NO can be added prior to the FTIR analyzer, which allows for the determination of the actual volumetric flow leaving the reactor and ensures a precise calculation of the product selectivities. Furthermore, additional N_2 can be dosed after the reactor to dilute the exhaust gas, hereby improving the signal-to-noise ratio of the FTIR data. As the MFCs are calibrated on a regular basis, their influence on the error within the analytics is considered low. Based on reference measurements, we estimated the error for the balances of the carbon and oxygen species generously around

±15% as a worst-case scenario. While the species balance may be biased by a poor signal-to-noise-ratio of the FTIR data, the absolute species concentration values measured under one operational point for the different catalyst samples are relatively similar (cf. Tables S5 and S6, Supplementary Information). Therefore, the error bars for a given operational point are fairly similar for different catalyst formulations and a reliable comparison regarding activity and selectivity is possible for the catalyst samples subject to the present study.

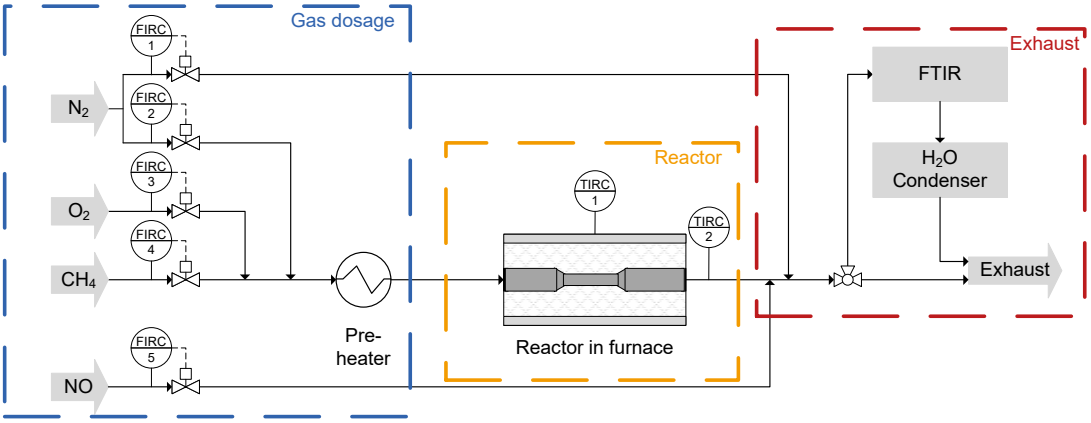

Figure 7. A schematic depiction of the used experimental setup divided into three parts: the gas dosage (**left**) with the gas supply system, the reactor (**middle**), and the exhaust system (**right**) with the analytics and the exhaust.

The experiments are mainly defined by three parameters: the gas hourly space velocity (GHSV), the nitrogen content in the stream (N_2 dilution), and the carbon to oxygen ratio in the feed (C:O ratio) that essentially defines the proportion of methane and oxygen. Preliminary tests were conducted in order to identify the most promising conditions where the catalysts subject to this study show high performance and run stable for at least 30 min per data point. Based on these pre-tests, the C:O ratio was kept constant at 0.55 throughout this study and space velocities of either 295,000 h^{-1} or 458,000 h^{-1} were chosen, while the N_2 dilution is varied from 80 vol.% to 40 vol.%. For the kinetic tests, the furnace is heated to 500 °C under nitrogen flow. Subsequently, the dosage of methane and oxygen as reactive gases while simultaneously reducing the N_2 content to 80 vol.% of the overall flow ignites the autothermal reaction. The share of reactive gases is increased in steps of 5 vol.%, while keeping the total flow rate constant by balancing with N_2. At each step, the reaction conditions are kept constant until a steady state was reached. An average of the last 2 min of the steady state of each relevant value (temperature, concentration, etc.) is the basis for the further evaluation. The results gathered at 50 vol.% nitrogen in the feed serve as reference point for evaluating the performance of the different catalysts.

4.3. Characterization Methods

For structural characterization of the prepared powder catalysts, N_2 physisorption was carried out with a BELSORP-mini II from BEL Japan (Tokyo, Japan). After degassing the sample for 2 h at 300 °C, the surface area of the samples was determined by the Brunauer–Emmett-Teller (BET) method [62] based on adsorption and desorption curves. A Bruker Advance D8 diffractometer (Bruker, Billerica, MA, USA) was used to record X-ray diffractograms of the fresh samples. Each data point was recorded using Cu-K_α radiation with a wavelength of 1.54 Å by scanning 2θ in 0.016° steps from 20° to 80° with an acquisition time of 0.51 s. For the analysis of the used samples, a PANalytical X'Pert Pro diffractometer was used. The diffractograms were recorded using Cu-K_α radiation with a step size of 0.017°, an acquisition time of 1 s, and a 2θ range from 20° to 80°. Prior to analyses of the spent samples, the washcoat was carefully scratched off the honeycomb substrate. Due to the dimensions of the monolithic catalyst samples, the amount of washcoat is limited, leading to a worse signal-to-noise ratio than for the fresh

catalyst samples and hindering a qualitative analysis. Elemental analysis of the Al, Pt, and dopant contents in the sample was carried out by inductively coupled plasma optical emission spectroscopy (ICP-OES) in an iCAP 7600 DUO analyzer (Thermo Fisher Scientific, Waltham, MA, USA) and confirmed the target loading for each specific catalyst formulation (cf. Supporting Information, Table S3). For the investigation of the spent samples after the kinetic measurements, the washcoat that was carefully scratched off the honeycomb was subject to analysis.

5. Conclusions

In order to reduce the noble metal loading while maintaining high catalytic activity and selectivity, our present study elucidates the role of dopants that can be added to platinum during the oxidative coupling of methane (OCM). For this, several bimetallic Pt-X catalysts, with X = Ni, Sn, and V_2O_5, were prepared in the weight ratios 3:1 and 1:3 with a total loading of 1 wt.% active material. After washcoating the received powder catalysts onto monolithic cordierite substrates, the catalyst samples were tested for their OCM performance. The monometallic 1 wt.% and 0.5 wt.% Pt/Al_2O_3 catalysts serve as references.

With respect to the C_2 selectivity, the dopants tested herein were found beneficial during OCM, most likely since they contribute to the catalyst system's capability in generating methyl radicals whose formation is a prerequisite for coupling reactions. Likewise, the dopants may promote (total) methane oxidation, which leads to higher temperatures that promote the formation of methyl radicals and thus C_2 species formation. Despite their significantly lower noble metal content, the addition of dopants to the catalyst formulation can even result in C_2 selectivities that exceed the performance of the 1 wt.% Pt/Al_2O_3 reference catalyst system. Measurements with a 0.5 wt.% Pt/Al_2O_3 catalyst underscore that the observed increase in selectivity during the OCM reactions cannot simply be attributed to a lower platinum amount but is indeed due to the dopant addition. Moreover, the evaluation of different Pt:X weight ratios reveals a beneficial effect of dopant addition even at Pt contents as low as 0.25 wt.%, which is a substantial reduction in the noble metal content compared to the reference catalyst containing 1 wt.% Pt.

In conclusion, our study uncovers that the addition of dopants can improve the overall C_2 selectivity of platinum-based catalytic systems during OCM while maintaining methane conversion at high levels. Since the usage of bimetallic systems allows for reducing the platinum content by up to three quarters, our study contributes to efforts in replacing expensive and scarce noble metals by non-noble metals in heterogeneous catalyst formulations and can hereby ease the dependency on precious metals. Likewise, certain non-noble metals, such as vanadium, may increase the stability of the Pt species under OCM conditions. Future studies may focus on the specific oxidation states of the used metal species, especially vanadium, to verify the assumptions made herein, as well as the *in situ* investigation of the formed species such as methyl radicals to optimize the operation conditions and catalyst composition. Ultimately, more advanced catalyst preparation techniques may exploit the findings presented in the present study in order to design and synthesize durable catalyst materials that are capable of withstanding the demanding and harsh OCM reaction conditions.

Supplementary Materials: The following supporting information can be downloaded at https://www.mdpi.com/article/10.3390/catal14110785/s1, Figure S1: Yield and downstream temperature versus the N_2 content in the feed of the 1 wt.% Pt/Al_2O_3 catalyst for (**A**) a GHSV of 458,000 h^{-1} and (**B**) a GHSV of 295,000 h^{-1}; Table S1: Methane conversion and product selectivities for all catalysts tested at a GHSV of 458,000 h^{-1}, a nitrogen content of 50% in the feed, and a C:O ratio of 0.55. Please note that the hydrogen content in the effluent gas stream was not directly measured but instead calculated via the hydrogen balance. Total active material loading of 1 wt.% for all bimetallic samples; Table S2: Methane conversion and product selectivities for all catalysts tested at a GHSV of 295,000 h^{-1}, a nitrogen content of 50% in the feed, and a C:O ratio of 0.55. Please note that the hydrogen content in the effluent gas stream was not directly measured but instead calculated via

the hydrogen balance; although the ethane selectivity was below 0.05% for all catalyst formulations subject to this study, it was still considered for calculating the total C_2 selectivity, e.g., resulting in a total C_2 selectivity of 11.3% for Pt-V_2O_5 (1:3). Total active material loading of 1 wt.% for all bimetallic samples; Table S3: Results from the ICP-OES analysis for the catalysts. The dopant content refers to the respective doped metal, if applicable; Figure S2: Comparison of the elemental analysis results for the catalysts before (left bar, darker color) and after (right bar, lighter color) usage with the Pt content in grey and the respective dopant content in green. Please note that for reasons of clarity, the oxygen content for the V_2O_5 species was added and that the processing of the 1 wt.% Pt/Al_2O_3 sample was faulty, therefore resulting in no usable data; Table S4: Results of the N_2 physisorption experiments. Both surface area and pore volume are determined with the BET method; Table S5: Absolute concentrations of the C_2 species determined by means of FTIR at a GHSV of 458,000 h^{-1}, a nitrogen content of 50% in the feed, and a C:O ratio of 0.55. Total active material loading of 1 wt.% for all bimetallic samples. Please note that the volume flow entering the FTIR is increased compared to the reactor exit flow rate due to a further dilution of the exhaust gas prior to the analytics; Table S6: Absolute concentrations of the C_2 species determined by means of FTIR at a GHSV of 295,000 h^{-1}, a nitrogen content of 50% in the feed, and a C:O ratio of 0.55. Total active material loading of 1 wt.% for all bimetallic samples. Please note that the volume flow entering the FTIR is increased compared to the reactor exit flow rate due to a further dilution of the exhaust gas prior to the analytics.

Author Contributions: Conceptualization, P.L.; methodology, S.S. and P.L.; validation, S.S.; formal analysis, S.S., S.B. and A.Ç.; investigation, S.S., S.B., A.Ç. and J.C.; resources, P.L.; data curation, S.S. and P.L.; writing—original draft preparation, S.S. and P.L.; writing—review and editing, J.C. and P.L.; visualization, S.S.; supervision, P.L.; project administration, P.L. All authors have read and agreed to the published version of the manuscript.

Funding: This research received no external funding.

Data Availability Statement: The original contributions presented in the study are included in the article/Supplementary Materials, and further inquiries can be directed to the corresponding author/s. The raw data supporting the conclusions of this article will be made available by the authors on request.

Acknowledgments: We thank O. Deutschmann for support regarding resources, infrastructure, and fruitful discussions; K. Urbschat for her support in preparing the catalysts; M. Makowiak for N_2 physisorption; and S. Struzek, A. de Giacinto (all ITCP, KIT) and D. Neukum (IKFT, KIT) for XRD measurements. Furthermore, we acknowledge T. Bergfeldt (IAM-AWP, KIT) for the elemental analysis and S. Schunk (hte GmbH/BASF SE) for fruitful discussions. The authors thank Corning for providing cordierite substrates and Sasol for the cost-free provision of Al_2O_3.

Conflicts of Interest: The authors declare no conflicts of interest.

References

1. Weiland, P. Biogas production: Current state and perspectives. *Appl. Microbiol. Biotechnol.* **2010**, *85*, 849–860. [CrossRef] [PubMed]
2. Schwach, P.; Pan, X.; Bao, X. Direct Conversion of Methane to Value-Added Chemicals over Heterogeneous Catalysts: Challenges and Prospects. *Chem. Rev.* **2017**, *117*, 8497–8520. [CrossRef]
3. Franz, R.; Uslamin, E.A.; Pidko, E.A. Challenges for the utilization of methane as a chemical feedstock. *Mendeleev Commun.* **2021**, *31*, 584–592. [CrossRef]
4. Hohn, K.L.; Witt, P.M.; Davis, M.B.; Schmidt, L.D. Methane coupling to acetylene over Pt-coated monoliths at millisecond contact times. *Catal. Lett.* **1998**, *54*, 113–118. [CrossRef]
5. Angeli, S.D.; Goßler, S.; Lichtenberg, S.; Kass, G.; Agrawal, A.K.; Valerius, M.; Kinzel, K.P.; Deutschmann, O. Reduction of CO_2 Emission from Off-Gases of Steel Industry by Dry Reforming of Methane. *Angew. Chem. Int. Ed.* **2021**, *60*, 11852–11857. [CrossRef]
6. Lott, P.; Mokashi, M.B.; Müller, H.; Heitlinger, D.J.; Lichtenberg, S.; Shirsath, A.B.; Janzer, C.; Tischer, S.; Maier, L.; Deutschmann, O. Hydrogen Production and Carbon Capture by Gas-Phase Methane Pyrolysis: A Feasibility Study. *ChemSusChem* **2023**, *16*, e202201720. [CrossRef]
7. Lott, P.; Deutschmann, O. Heterogeneous chemical reactions—A cornerstone in emission reduction of local pollutants and greenhouse gases. *Proc. Combust. Inst.* **2023**, *39*, 3183–3215. [CrossRef]
8. Horn, R.; Schlögl, R. Methane Activation by Heterogeneous Catalysis. *Catal. Lett.* **2015**, *145*, 23–39. [CrossRef]
9. Halser, C.; Paraschiv, F. Pathways to Overcoming Natural Gas Dependency on Russia—The German Case. *Energies* **2022**, *15*, 4939. [CrossRef]
10. Ghaib, K.; Ben-Fares, F.-Z. Power-to-Methane: A state-of-the-art review. *Renew. Sustain. Energy Rev.* **2018**, *81*, 433–446. [CrossRef]

11. Deutschmann, O.; Schmidt, L.D. Modeling the partial oxidation of methane in a short-contact-time reactor. *AIChE J.* **1998**, *44*, 2465–2477. [CrossRef]
12. Bitsch-Larsen, A.; Horn, R.; Schmidt, L.D. Catalytic partial oxidation of methane on rhodium and platinum: Spatial profiles at elevated pressure. *Appl. Catal. A* **2008**, *348*, 165–172. [CrossRef]
13. Pietrogiacomi, D.; Campa, M.C.; Pettiti, I.; Tuti, S.; Luccisano, G.; Ardemani, L.; Luisetto, I.; Gazzoli, D. Oscillatory Behaviour of Ni Supported on ZrO_2 in the Catalytic Partial Oxidation of Methane as Determined by Activation Procedure. *Materials* **2021**, *14*, 2495. [CrossRef]
14. Vella, L.D.; Specchia, S. Alumina-supported nickel catalysts for catalytic partial oxidation of methane in short-contact time reactors. *Catal. Today* **2011**, *176*, 340–346. [CrossRef]
15. Schwiedernoch, R.; Tischer, S.; Correa, C.; Deutschmann, O. Experimental and numerical study on the transient behavior of partial oxidation of methane in a catalytic monolith. *Chem. Eng. Sci.* **2003**, *58*, 633–642. [CrossRef]
16. Schmidt, L.D.; Hohn, K.L.; Davis, M.B. Catalytic Partial Oxidation of Methane at Extremely Short Contact Times: Production of Acetylene. *Stud. Surf. Sci. Catal.* **1998**, *119*, 397–402. [CrossRef]
17. Liu, J.; Yue, J.; Lv, M.; Wang, F.; Cui, Y.; Zhang, Z.; Xu, G. From fundamentals to chemical engineering on oxidative coupling of methane for ethylene production: A review. *Carbon Resour. Convers.* **2022**, *5*, 1–14. [CrossRef]
18. Keller, G.E.; Bhasin, M.M. Synthesis of ethylene via oxidative coupling of methane I. Determination of active catalysts. *J. Catal.* **1982**, *73*, 9–19. [CrossRef]
19. Chawla, J.; Schardt, S.; Angeli, S.D.; Lott, P.; Tischer, S.; Maier, L.; Deutschmann, O. Oxidative Coupling of Methane over Pt/Al_2O_3 at High Temperature: Multiscale Modeling of the Catalytic Monolith. *Catalysts* **2022**, *12*, 189. [CrossRef]
20. Lunsford, J.H. The Catalytic Oxidative Coupling of Methane. *Angew. Chem. Int. Ed.* **1995**, *34*, 970–980. [CrossRef]
21. Zhou, Q.; Wang, Z.-Q.; Li, Z.; Wang, J.; Xu, M.; Zou, S.; Yang, J.; Pan, Y.; Gong, X.-Q.; Xiao, L.; et al. $CH_3^{\bullet}$-Generating Capability as a Reactivity Descriptor for Metal Oxides in Oxidative Coupling of Methane. *ACS Catal.* **2021**, *11*, 14651–14659. [CrossRef]
22. Kim, M.; Arndt, S.; Yildiz, M.; Schomäcker, R.; Görke, O.; Repke, J.-U.; Wozny, G.; Godini, H.R. Reaction engineering of oxidative coupling of methane. *Chem. Eng. Res. Des.* **2021**, *172*, 84–98. [CrossRef]
23. Arndt, S.; Otremba, T.; Simon, U.; Yildiz, M.; Schubert, H.; Schomäcker, R. $Mn–Na_2WO_4/SiO_2$ as catalyst for the oxidative coupling of methane. What is really known? *Appl. Catal. A* **2012**, *425–426*, 53–61. [CrossRef]
24. Serres, T.; Aquino, C.; Mirodatos, C.; Schuurman, Y. Influence of the composition/texture of Mn–Na–W catalysts on the oxidative coupling of methane. *Appl. Catal. A* **2015**, *504*, 509–518. [CrossRef]
25. Ortiz-Bravo, C.A.; Chagas, C.A.; Toniolo, F.S. Oxidative coupling of methane (OCM): An overview of the challenges and opportunities for developing new technologies. *J. Nat. Gas Sci. Eng.* **2021**, *96*, 104254. [CrossRef]
26. Noon, D.; Zohour, B.; Senkan, S. Oxidative coupling of methane with $La_2O_3–CeO_2$ nanofiber fabrics: A reaction engineering study. *J. Nat. Gas Sci. Eng.* **2014**, *18*, 406–411. [CrossRef]
27. Tonkovich, A.L.; Carr, R.W.; Aris, R. Enhanced C_2 yields from methane oxidative coupling by means of a separative chemical reactor. *Science* **1993**, *262*, 221–223. [CrossRef]
28. Zavyalova, U.; Geske, M.; Horn, R.; Weinberg, G.; Frandsen, W.; Schuster, M.E.; Schlögl, R. Morphology and Microstructure of Li/MgO Catalysts for the Oxidative Coupling of Methane. *ChemCatChem* **2011**, *3*, 949–959. [CrossRef]
29. Wang, K.; Ji, S.; Shi, X.; Tang, J. Autothermal oxidative coupling of methane on the $SrCO_3/Sm_2O_3$ catalysts. *Catal. Commun.* **2009**, *10*, 807–810. [CrossRef]
30. Cavani, F.; Ballarini, N.; Cericola, A. Oxidative dehydrogenation of ethane and propane: How far from commercial implementation? *Catal. Today* **2007**, *127*, 113–131. [CrossRef]
31. Claycomb, G.D.; Sherwood, P.M.A.; Traxel, B.E.; Hohn, K.L. X-ray Photoelectron Spectroscopic Study of the Surface State during Ethane Oxidative Dehydrogenation at Millisecond Contact Times. *J. Phys. Chem. C* **2007**, *111*, 18724–18730. [CrossRef]
32. Huff, M.C.; Schmidt, L.D. Ethylene formation by oxidative dehydrogenation of ethane over monoliths at very short contact times. *J. Phys. Chem.* **1993**, *97*, 11815–11822. [CrossRef]
33. Yokoyama, C.; Bharadwaj, S.S.; Schmidt, L.D. Platinum-tin and platinum-copper catalysts for autothermal oxidative dehydrogenation of ethane to ethylene. *Catal. Lett.* **1996**, *38*, 181–188. [CrossRef]
34. Chawla, J.; Schardt, S.; Lott, P.; Angeli, S.; Tischer, S.; Maier, L.; Deutschmann, O. Detailed kinetic modeling of catalytic oxidative coupling of methane. *Chem. Eng. J.* **2024**, *482*, 148719. [CrossRef]
35. Schardt, S.; Ehrlich, F.; Lott, P. Autothermal Oxidative Coupling of Methane over Pt/Al_2O_3 Catalysts Doped with Rare Earth Oxides. *Chem. Ing. Tech.* **2024**, *96*, 840–849. [CrossRef]
36. Pääkkönen, A.; Tolvanen, H.; Kokko, L. The economics of renewable CaC_2 and C_2H_2 production from biomass and CaO. *Biomass Bioenergy* **2019**, *120*, 40–48. [CrossRef]
37. Shlyapin, D.A.; Afonasenko, T.N.; Glyzdova, D.V.; Leont'eva, N.N.; Lavrenov, A.V. Acetylene Production Technologies in the 21st Century: Main Trends of Their Development in the Paradigm of Low-Carbon Economy of the Future. *Catal. Ind.* **2022**, *14*, 251–267. [CrossRef]
38. Abdelbaki, Y.; de Arriba, A.; Solsona, B.; Delgado, D.; García-González, E.; Issaadi, R.; López Nieto, J.M. The nickel-support interaction as determining factor of the selectivity to ethylene in the oxidative dehydrogenation of ethane over nickel oxide/alumina catalysts. *Appl. Catal. A* **2021**, *623*, 118242. [CrossRef]

39. Koranne, M.M.; Goodwin, J.G.; Marcelin, G. Oxygen Involvement in the Partial Oxidation of Methane on Supported and Unsupported V_2O_5. *J. Catal.* **1994**, *148*, 378–387. [CrossRef]
40. Ross, J.R. Nickel Catalysts for C_1 Reactions: Recollections from a Career in Heterogeneous Catalysis. *Top. Catal.* **2021**, *64*, 896–906. [CrossRef]
41. Korf, S.J.; Roos, J.A.; Vreeman, J.A.; Derksen, J.; van Ommen, J.G.; Ross, J.R. A study of the kinetics of the oxidative coupling of methane over a Li/Sn/MgO catalyst. *Catal. Today* **1990**, *6*, 417–426. [CrossRef]
42. Dang, Z.; Gu, J.; Lin, J.; Yang, D. $BaCO_3$-supported vanadium oxide catalysts for the oxidative coupling of methane. *Chem. Commun.* **1996**, *16*, 1901–1902. [CrossRef]
43. Holleman, A.F.; Wiberg, E.; Wiberg, N. *Lehrbuch der Anorganischen Chemie*; Walter de Gruyter: Berlin, Germany, 2007; ISBN 9783110206845.
44. Gusmão, C.d.A.; Borges, L.T.; Palharim, P.H.; Otubo, L.; Rodrigues, O.; Gouvea, D.; Ramos, B.; Teixeira, A.C.S.C. Synthesis, Characterization, and Application of Pt/PtO_2-TiO_2/SiO_2 Materials on a Continuous Flow Packed Bed Microreactor for Enhanced Photocatalytic Activity under Sunlight. *Water* **2022**, *14*, 3864. [CrossRef]
45. Savchenko, V.I.; Zimin, Y.S.; Nikitin, A.V.; Sedov, I.V.; Arutyunov, V.S. Non-Catalytic Steam Reforming of C_1–C_4 Hydrocarbons. *Pet. Chem.* **2021**, *61*, 762–772. [CrossRef]
46. Weckhuysen, B.M.; Keller, D.E. Chemistry, spectroscopy and the role of supported vanadium oxides in heterogeneous catalysis. *Catal. Today* **2003**, *78*, 25–46. [CrossRef]
47. Jansson, J. Vanadia-Based Catalysts for Mobile SCR. In *Urea-SCR Technology for deNOx After Treatment of Diesel Exhausts*; Nova, I., Tronconi, E., Eds.; Springer: New York, NY, USA, 2014; pp. 65–96, ISBN 978-1-4899-8070-0.
48. Lott, P.; Wagner, U.; Koch, T.; Deutschmann, O. Hydrogen Combustion Engines—Chances and Challenges on the Way Towards a Decarbonized Mobility. *Chem. Ing. Tech.* **2022**, *94*, 217–229. [CrossRef]
49. Tronconi, E.; Nova, I.; Ciardelli, C.; Chatterjee, D.; Weibel, M. Redox features in the catalytic mechanism of the "standard" and "fast" NH_3-SCR of NO_x over a V-based catalyst investigated by dynamic methods. *J. Catal.* **2007**, *245*, 1–10. [CrossRef]
50. Harlin, M.E.; Niemi, V.M.; Krause, A. Alumina-Supported Vanadium Oxide in the Dehydrogenation of Butanes. *J. Catal.* **2000**, *195*, 67–78. [CrossRef]
51. Trunschke, A.; Noack, J.; Trojanov, S.; Girgsdies, F.; Lunkenbein, T.; Pfeifer, V.; Hävecker, M.; Kube, P.; Sprung, C.; Rosowski, F.; et al. The Impact of the Bulk Structure on Surface Dynamics of Complex Mo–V-based Oxide Catalysts. *ACS Catal.* **2017**, *7*, 3061–3071. [CrossRef]
52. Chapman, D.M. Behavior of titania-supported vanadia and tungsta SCR catalysts at high temperatures in reactant streams: Tungsten and vanadium oxide and hydroxide vapor pressure reduction by surficial stabilization. *Appl. Catal. A* **2011**, *392*, 143–150. [CrossRef]
53. Rodriguez-Gomez, A.; Chowdhury, A.D.; Caglayan, M.; Bau, J.A.; Abou-Hamad, E.; Gascon, J. Non-oxidative dehydrogenation of isobutane over supported vanadium oxide: Nature of the active sites and coke formation. *Catal. Sci. Technol.* **2020**, *10*, 6139–6151. [CrossRef]
54. Hu, S.; Herner, J.D.; Shafer, M.; Robertson, W.; Schauer, J.J.; Dwyer, H.; Collins, J.; Huai, T.; Ayala, A. Metals emitted from heavy-duty diesel vehicles equipped with advanced PM and NO_X emission controls. *Atmos. Environ.* **2009**, *43*, 2950–2959. [CrossRef]
55. Angeli, S.D.; Monteleone, G.; Giaconia, A.; Lemonidou, A.A. State-of-the-art catalysts for CH_4 steam reforming at low temperature. *Int. J. Hydrogen Energy* **2014**, *39*, 1979–1997. [CrossRef]
56. Zhu, T.; van Grootel, P.W.; Filot, I.A.W.; Sun, S.-G.; van Santen, R.A.; Hensen, E.J.M. Microkinetics of steam methane reforming on platinum and rhodium metal surfaces. *J. Catal.* **2013**, *297*, 227–235. [CrossRef]
57. Du, Y.; Zou, J.; Guo, Y.; Xu, X.; Chen, H.; Su, C.; Zeng, Z.; Li, L. A novel viewpoint on the surface adsorbed oxygen and the atom doping in the catalytic oxidation of toluene over low-Pt bimetal catalysts. *Appl. Catal. A* **2021**, *609*, 117913. [CrossRef]
58. Marceau, E.; Che, M.; Saint-Just, J.; Tatibouët, J.M. Influence of chlorine ions in Pt/Al_2O_3 catalysts for methane total oxidation. *Catal. Today* **1996**, *29*, 415–419. [CrossRef]
59. García-Diéguez, M.; Pieta, I.S.; Herrera, M.C.; Larrubia, M.A.; Malpartida, I.; Alemany, L.J. Transient study of the dry reforming of methane over Pt supported on different γ-Al_2O_3. *Catal. Today* **2010**, *149*, 380–387. [CrossRef]
60. Rocha, K.O.; Santos, J.; Meira, D.; Pizani, P.S.; Marques, C.; Zanchet, D.; Bueno, J. Catalytic partial oxidation and steam reforming of methane on La_2O_3–Al_2O_3 supported Pt catalysts as observed by X-ray absorption spectroscopy. *Appl. Catal. A* **2012**, *431–432*, 79–87. [CrossRef]
61. Karinshak, K.A.; Lott, P.; Harold, M.P.; Deutschmann, O. In situ Activation of Bimetallic Pd−Pt Methane Oxidation Catalysts. *ChemCatChem* **2020**, *12*, 3712–3720. [CrossRef]
62. Brunauer, S.; Emmett, P.H.; Teller, E. Adsorption of Gases in Multimolecular Layers. *J. Am. Chem. Soc.* **1938**, *60*, 309–319. [CrossRef]

Disclaimer/Publisher's Note: The statements, opinions and data contained in all publications are solely those of the individual author(s) and contributor(s) and not of MDPI and/or the editor(s). MDPI and/or the editor(s) disclaim responsibility for any injury to people or property resulting from any ideas, methods, instructions or products referred to in the content.